Incorporation of Mo into the vacant T-atom sites of the framework of BEA zeolite as mononuclear Mo evidenced by XRD and FTIR, NMR, EPR, and DR UV-vis spectroscopies

ARTICLE *in* THE JOURNAL OF PHYSICAL CHEMISTRY C · FEBRUARY 2014

Impact Factor: 4.77 · DOI: 10.1021/jp410016g

6 AUTHORS, INCLUDING:

Rafal Baran
European Synchrotron Radiation Facility
16 PUBLICATIONS **76** CITATIONS
SEE PROFILE

Thomas Onfroy
Pierre and Marie Curie University - Paris 6
40 PUBLICATIONS **503** CITATIONS
SEE PROFILE

Sandra Casale
Pierre and Marie Curie University - Paris 6
71 PUBLICATIONS **280** CITATIONS
SEE PROFILE

Stanislaw Dzwigaj
Pierre and Marie Curie University - Paris 6
116 PUBLICATIONS **1,749** CITATIONS
SEE PROFILE

THE JOURNAL OF PHYSICAL CHEMISTRY C

Article

pubs.acs.org/JPCC

Incorporation of Mo into the Vacant T-Atom Sites of the Framework of BEA Zeolite as Mononuclear Mo Evidenced by XRD and FTIR, NMR, EPR, and DR UV−Vis Spectroscopies

Rafal Baran,[†,‡,§] Frederic Averseng,[†,‡] Yannick Millot,[†,‡] Thomas Onfroy,[†,‡] Sandra Casale,[†,‡] and Stanislaw Dzwigaj*[,†,‡]

[†]Laboratoire de Réactivité de Surface, Sorbonne Universités, UPMC Université Paris 06, UMR 7197, F-75005 Paris, France

[‡]Laboratoire de Réactivité de Surface, CNRS, UMR 7197, F-75005 Paris, France

[§]Faculty of Energy and Fuels, AGH University of Science and Technology, Aleja Adama Mickiewicza 30, 30-059 Krakow, Poland

ABSTRACT: A MoSiBEA zeolite has been prepared by a two-step postsynthesis procedure that consists of first creating the vacant T-atom sites with associated silanol groups by treatment of TEABEA zeolite with nitric acid and then incorporating Mo ions into the vacant T-atom sites by solid-state ion exchange at 773 K using molybdenum(II) acetate. The incorporation of Mo ions into the vacant T-atom sites of the framework of SiBEA zeolite as isolated mononuclear Mo(VI) species was evidenced by the combined use of XRD and FTIR, NMR, and diffuse reflectance UV−visible spectroscopies. The consumption of OH groups was monitored by FTIR spectroscopy. The reducibility of Mo was investigated by TPR and EPR spectroscopy. The size of very small well-dispersed Mo(0) nanoparticles formed upon treatment of MoSiBEA between 298 and 1240 K in hydrogen stream (5% H_2/Ar) was measured by TEM.

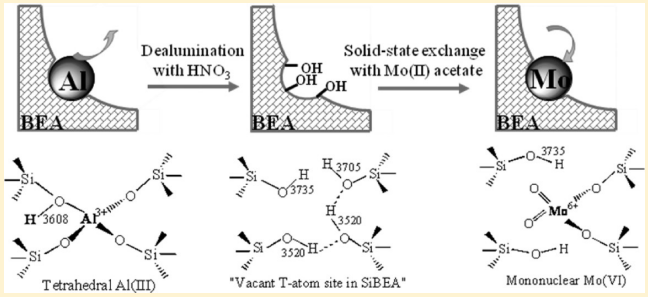

1. INTRODUCTION

Molybdenum-containing materials are widely applied as catalysts in industrial processes such as hydrodesulfurization and hydrodenitrogenation,[1] toluene hydrogenation,[2] olefin methathesis,[3] methane transformation into aromatic hydrocarbons,[4,5] and methanol oxidation.[6] The method often used for Mo introduction into oxide supports is wet impregnation with application of ammonium heptamolybdate as a Mo precursor, followed by calcination[7,8] and ion exchange.[9] However, a major problem with this method is its nonselectivity, resulting in the introduction of metals in the form of various species such as isolated framework and extraframework metal species, metal oligomers, and/or metal oxides. Therefore, other methods such as vapor-phase deposition,[10,11] sol−gel synthesis,[12] and solid-state ion exchange[12] have been tested for the preparation of well-dispersed Mo-containing materials.

In addition, this problem can be solved by application of the two-step postsynthesis procedure recently developed by Dzwigaj et al.,[14−17] which consists of first creating the vacant T-atom sites by treating tetraethylammonium BEA (TEABEA) zeolite with nitric acid and then incorporating metal ions into vacant T-atom sites of resulting SiBEA by their reaction with silanol nests. As shown earlier,[15−18] for low metal content (<2 wt %), this postsynthesis procedure allows metal ions to be incorporated mainly as isolated species without the formation of metal oligomers or metal oxide. Thus, in the present work, we have used a molybdenum precursor [molybdenum(II) acetate] and the two-step postsynthesis procedure described above to incorporate molybdenum into the framework of BEA zeolite.

The incorporation of molybdenum into the vacant T-atom sites of BEA zeolite as isolated mononuclear Mo species was evidenced by X-ray diffraction (XRD); Fourier transform infrared (FTIR), nuclear magnetic resonance (NMR), diffuse-reflectance UV−visible (DR UV−vis), and electron paramagnetic resonance (EPR) spectroscopies; and temperature-programmed reduction (TPR).

2. EXPERIMENTAL SECTION

2.1. Materials. A tetraethylammonium BEA (TEABEA) zeolite with a Si/Al atomic ratio of 17 provided by RIPP (China) was separated into two fractions. The first fraction of TEABEA was calcined in air at 823 K for 15 h under static conditions to remove the organic template and to obtain the organic-free zeolite, denoted as HAlBEA.

The second fraction of TEABEA zeolite was dealuminated by a treatment with nitric acid solution (c = 13 mol L^{-1}) at 353 K for 4 h, to obtain SiBEA with an atomic Si/Al ratio of 1500 and then washed several times with distilled water and dried at 368 K overnight.

Received: October 8, 2013
Revised: February 5, 2014
Published: February 14, 2014

   dx.doi.org/10.1021/jp410016g | J. Phys. Chem. C 2014, 118, 4143−4150

SiBEA zeolite and molybdenum(II) acetate with the desired amount of Mo (1 or 2 Mo wt % in Mo-containing SiBEA) were ground and mixed in an agate mortar for 15 min. The obtained mixture was transferred to a glass reactor and heated in flowing argon (150 mL min^{-1}) to 773 K at a heating rate of 2 K min^{-1} and held at this temperature for 12 h. After that, the gas flow was changed from argon to O_2, and the solids were calcined at 773 K for 3 h. The as-obtained Mo-containing SiBEA materials are labeled $Mo_{1.0}$SiBEA and $Mo_{2.0}$SiBEA.

2.2. Techniques. X-ray fluorescence (XRF) chemical analysis was performed at room temperature on a SPECTRO X-LabPro apparatus.

XRD patterns were recorded at room temperature on a Bruker D8 Advance diffractometer using the Cu Kα radiation (λ = 154.05 pm)

Specific surface areas and nitrogen adsorption isotherms at 77 K were measured on an ASAP 2010 apparatus (Micromeritics). All samples were outgassed, first at room temperature and then at 623 K to a pressure <0.2 Pa. The surface areas were determined from nitrogen adsorption values for five relative pressures (P/P_0) ranging from 0.05 to 0.16 using the Brunauer–Emmett–Teller (BET) method. The volume of micropores was determined from the amount of N_2 adsorbed up to P/P_0 = 0.2.

Before FTIR experiments, the wafers were activated by calcination under static conditions at 723 K for 3 h in O_2 (1.6×10^4 Pa) and then outgassed under a secondary vacuum at 573 K (10^{-3} Pa) for 1 h. FTIR spectra were recorded with a Bruker Vector 22 spectrometer (resolution 2 cm^{-1}, 128 scans). All spectra were normalized before comparison with each other.

^{1}H magic-angle-spinning (MAS) NMR spectra were recorded on a Bruker Avance 500 spectrometer at 500 MHz with a 90° pulse duration of 3 μs and a recycle delay of 5 s. To record only the proton signal of the sample, the equipment for rotation (12 kHz) was carefully cleaned with ethanol and dried in air at room temperature. The proton signals from the probe and rotor were subtracted from the total free induction decay.

DR UV–vis spectra were recorded at ambient atmosphere on a Cary 5000 Varian spectrometer equipped with a double integrator with polytetrafluoroethylene as the reference.

EPR spectra were recorded on a JEOL FA-300 series EPR spectrometer at ~9.3 GHz (X band) using a 100-kHz field modulation and a 5–10-G standard modulation width. The spectra were recorded at 298 and 77 K. The $Mo_{1.0}$SiBEA sample was treated at 773 K for 2 h under a dynamic vacuum of 10^{-3} Pa, which leads to the activated sample Act-$Mo_{1.0}$SiBEA, and then this activated sample was treated with H_2 at 943 K for 1 h, leading to the sample Red-Act-$Mo_{1.0}$SiBEA.

Simulations were performed using the EPRSim32 software developed by Spalek et al.[19] For the simulations, two Mo isotope categories were considered: (1) ^{92,94,96,98,100}Mo (I = 0) with a combined natural abundance of 74.5% and (2) ^{95}Mo (I = $^5/_2$) and ^{97}Mo (I = $^5/_2$) with a combined natural abundance of 25.5% (15.9% + 9.6%, respectively). The simulated hyperfine coupling constant values ($A_\perp$ and $A_\parallel$) were obtained considering similar g_n values for the ^{95}Mo and ^{97}Mo isotopes. The estimated uncertainties in simulated parameters are ±0.005 for g and ±15 G for A.

H_2 TPR measurements were carried out on an AutoChem 2910 apparatus (Micromeritics) in the temperature range of 298–1240 with a linear heating rate of 7 K min^{-1}. Samples (about 0.1 g) were reduced in hydrogen stream (5% H_2/Ar) with a gas volume velocity of 40 cm^3 min^{-1}. Hydrogen consumption was monitored with a thermal conductivity detector (TCD).

A transmission electron microscopy (TEM) study of $Mo_{2.0}$SiBEA after treatment in flowing mixture 5% H_2/Ar with a linear heating rate 7 K min^{-1} from 298 to 1240 K was carried out using a JEOL JEM-100CXII electron microscope operated at an acceleration voltage of 100 keV. The samples were prepared by dispersing them in pure alcohol using ultrasonic cleaner and putting a drop of this suspension on carbon films on copper grids.

3. RESULTS AND DISCUSSION

3.1. XRD and FTIR Evidence for the Incorporation of Molybdenum into the Framework of SiBEA. Results of XRF chemical analysis indicate that nitric acid treatment almost completely removed aluminum ions from zeolite BEA. The Si/Al ratio of SiBEA was >1500, and only traces of Al were present after the dealumination step (Table 1). The XRF chemical analysis of Mo_xSiBEA samples was repeated three times and allowed the determination of 1 or 2 wt % Mo in the samples labeled $Mo_{1.0}$SiBEA and $Mo_{2.0}$SiBEA, respectively.

Table 1. XRF Chemical Analysis of HAlBEA, SiBEA, $Mo_{1.0}$SiBEA, and $Mo_{2.0}$SiBEA

sample	Mo (wt %)	Si/Al ratio
HAlBEA	0	17
SiBEA	0	>1500
$Mo_{1.0}$SiBEA	0.7	>1500
$Mo_{2.0}$SiBEA	1.98	>1500

The X-ray diffractograms of HAlBEA and SiBEA were found to be similar (Figure 1), suggesting that the dealumination does not significantly affect the structure of the zeolite. Although the determination of the unit cell parameters in BEA zeolite is difficult because of the coexistence of several polytypes,[20−22] it is still possible to obtain information on the contraction/

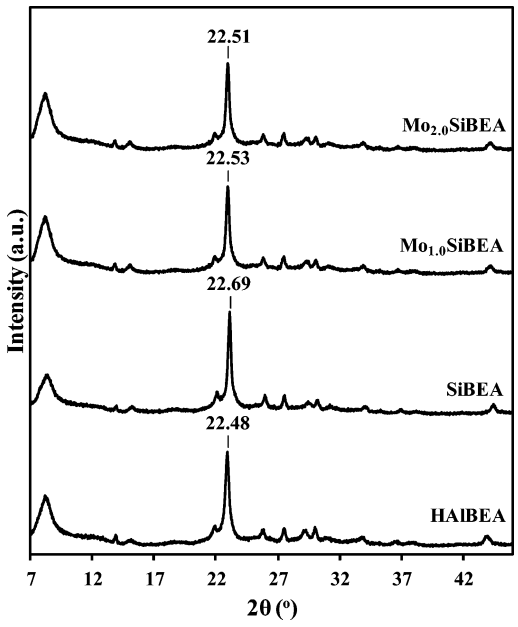

Figure 1. XRD patterns of HAlBEA, SiBEA, $Mo_{1.0}$SiBEA, and $Mo_{2.0}$SiBEA recorded at room temperature.

dx.doi.org/10.1021/jp410016g | J. Phys. Chem. C 2014, 118, 4143–4150

expansion of the zeolite matrix from the position of the diffraction peak (302) at 2θ = 22.5−22.6°, within a given series of zeolite samples.[23−25] The d_{302} spacing, calculated from the corresponding 2θ value, decreased from 3.950 (HAlBEA) (with 2θ = 22.48°) to 3.914 Å (SiBEA) (with 2θ = 22.69°), suggesting a matrix contraction, consistent with the removal of aluminum.[22]

As shown in Figure 2 and Table 2, the nitrogen adsorption/desorption isotherms of HAlBEA, SiBEA, $Mo_{1.0}$SiBEA, and $Mo_{2.0}$SiBEA can be classified as type I according to IUPAC. HAlBEA, SiBEA, $Mo_{1.0}$SiBEA, and $Mo_{2.0}$SiBEA were found to have similar BET surface areas (613−773 m^2 g^{-1}) and micropore volumes (0.25−0.31 mL g^{-1}), indicating that the textural properties of BEA zeolite were preserved and there was no formation of mesoporosity upon dealumination of BEA zeolite and incorporation of molybdenum atoms into SiBEA.

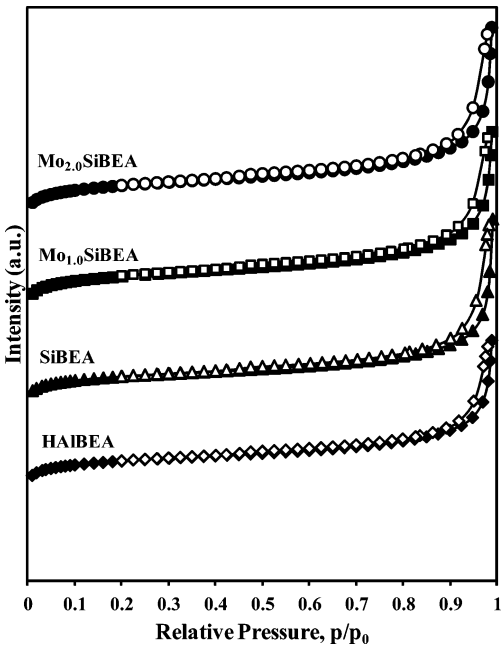

Figure 2. Isotherms of nitrogen adsorption at 77 K on HAlBEA, SiBEA, $Mo_{1.0}$SiBEA, and $Mo_{2.0}$SiBEA. Solid symbols, adsorption; open symbols, desorption. For convenience, the data sets for SiBEA, $Mo_{1.0}$SiBEA, and $Mo_{2.0}$SiBEA are shifted upward along the y axis.

Table 2. Textural Properties of HAlBEA, SiBEA, $Mo_{1.0}$SiBEA, and $Mo_{2.0}$SiBEA

sample	specific surface area, S_{BET} (m^2 g^{-1})	micropore volume, V_{mic} (cm^3 g^{-1})
HAlBEA	626	0.26
SiBEA	613	0.25
$Mo_{1.0}$SiBEA	770	0.31
$Mo_{2.0}$SiBEA	773	0.31

The FTIR spectrum of HAlBEA exhibits six IR bands (Figure 3), attributed to AlO—H groups (3781 and 3660 cm^{-1}), bridging acidic hydroxyls Si—O(H)—Al (3608 cm^{-1}),[26,27] isolated external SiO—H groups (with a narrow band at 3745 cm^{-1}), isolated internal SiO—H groups (shoulder at 3735 cm^{-1}), and hydrogen-bonded SiO—H groups (a broad band at 3540 cm^{-1}).[28] Upon treatment of HAlBEA with concentrated nitric acid, the three bands at 3781, 3660, and 3608 cm^{-1} related to AlO—H and Si—O(H)—Al groups disappeared,

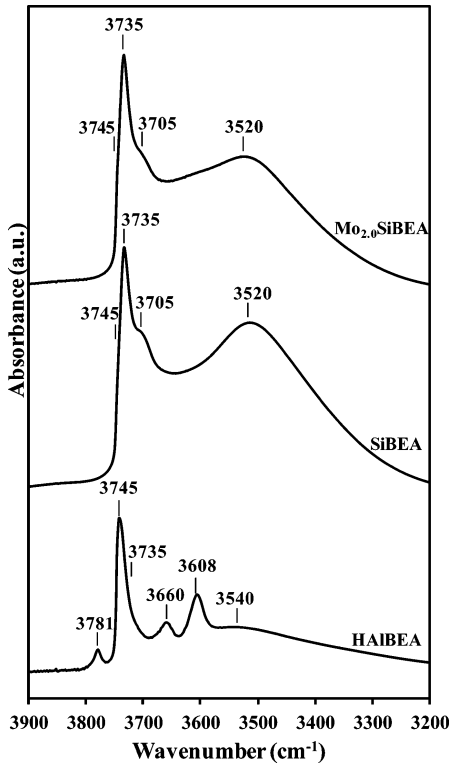

Figure 3. Room-temperature FTIR spectra of HAlBEA, SiBEA, and $Mo_{2.0}$SiBEA in the vibrational range of the OH group.

suggesting that aluminum was removed from the BEA structure. The appearance of the intense IR bands at 3735 and 3705 cm^{-1} related to isolated internal and terminal internal silanol groups and the broad band of H-bonded SiO—H groups at 3520 cm^{-1} (Figure 3) reveal the creation of vacant T-atom sites associated with silanol groups upon the removal of framework aluminum, as shown in Scheme 1.

Upon introduction of Mo into SiBEA, the d_{302} spacing, related to the narrow main diffraction peak near 22.6°, increased from 3.914 Å (SiBEA) (with 2θ = 22.69°) to 3.942 Å ($Mo_{1.0}$SiBEA) (with 2θ = 22.53°) and to 3.945 Å ($Mo_{2.0}$SiBEA) (with 2θ = 22.51°) (Figure 1). This increase can be taken as evidence of framework expansion of the BEA structure and suggests the incorporation of molybdenum atoms into the vacant-T-atom sites of the framework of SiBEA zeolite, in line with earlier reports for VSiBEA zeolites.[16]

The incorporation of molybdenum into SiBEA leads to a decrease of the intensity of the IR bands at 3735, 3705, and 3520 cm^{-1} of isolated internal, terminal internal, and hydrogen-bonded SiO—H groups (Figure 3), suggesting that these silanol groups react with the Mo precursor, as proposed in Scheme 1. To the best of our knowledge, this is the first time that molybdenum has been incorporated into the vacant T-atom sites of the framework of BEA zeolite, which might be very important for the catalytic application of such materials.

The incorporation of molybdenum atoms into the vacant T-atom sites was confirmed by ^{1}H MAS NMR spectroscopy. As shown in Figure 4, the spectrum of SiBEA exhibits several intense peaks at the range of 1−4 ppm due to the protons of isolated internal, terminal internal, and H-bonded SiO—H groups present in the vacant-T-atom sites, in line with earlier data on BEA and MFI zeolites.[29,30] The disappearance of the peaks at 1.2 and 3.2 ppm and the significant decrease of the

dx.doi.org/10.1021/jp410016g | J. Phys. Chem. C 2014, 118, 4143−4150

Scheme 1. Schematic Representation of Hydroxyl Nest Formation within the Vacant T-Atom Sites Created by Dealumination of TEABEA Zeolites in the First Step of the Postsynthesis Process[a] and Incorporation of Mo into Vacant T-Atom Sites in the Second Step[b]

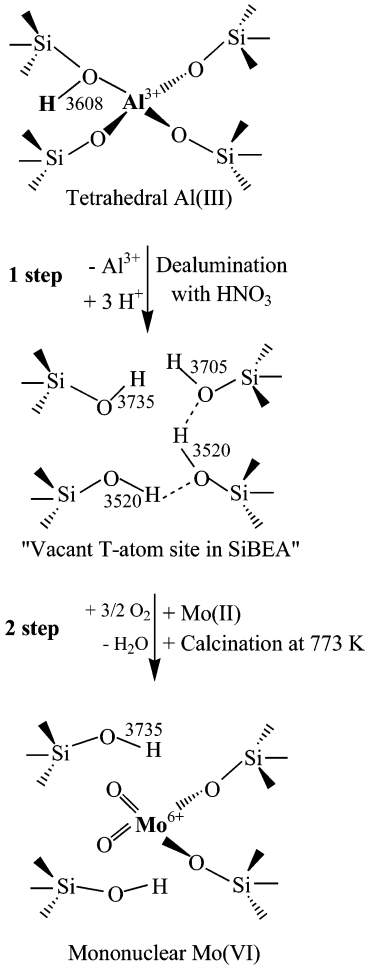

[a]See text. [b]Numbers quoted correspond to wavenumbers, with values of 3735, 3705, 3608, and 3520 cm^{-1} corresponding to isolated internal SiO—H, terminal internal SiO—H, Al—O(H)—Si, and H-bonded SiO—H vibrators, respectively.

intensity of the peak at 3.9 ppm upon incorporation of Mo into SiBEA (Figure 4) provide evidence for the reaction of the molybdenum precursor with the SiO—H groups of the vacant T-atom sites.

3.2. DR UV−Vis Evidence for the Formation of Isolated Mononuclear Mo(VI). The nature and environment of the Mo in Mo_xSiBEA were investigated by DR UV−vis spectroscopy. Figure 5 shows the DR UV−vis spectra of $Mo_{1.0}$SiBEA and $Mo_{2.0}$SiBEA. For both samples, two bands at 265 and 320 nm appear whose intensity increases simultaneously with Mo content, indicating that molybdenum occurs in $Mo_{1.0}$SiBEA and $Mo_{2.0}$SiBEA as well-dispersed mononuclear Mo species, in line with earlier works on molybdenum-containing materials.[5,31−36] The simultaneous increasing of the intensities of the bands at 265 and 320 nm with Mo content (Figure 5) and the wavelengths of these bands suggest that both bands are probably attributable to oxygen-to-mononuclear Mo(VI) charge-transfer transitions involving oxygen in bridging (Mo−O−Si) and terminal (Mo═O) positions, respectively

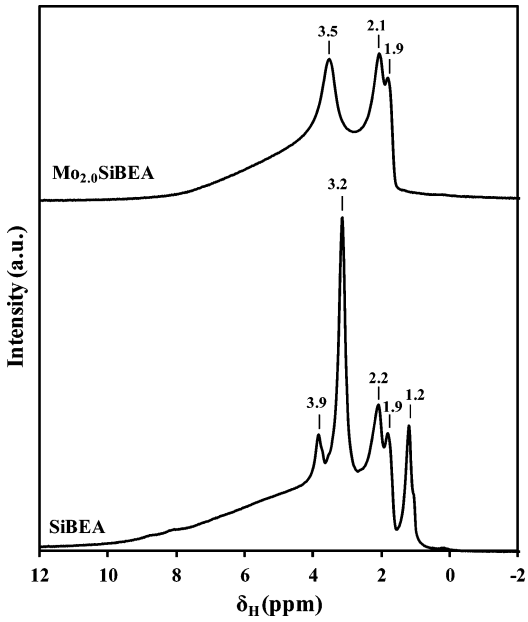

Figure 4. Room-temperature ^{1}H MAS NMR spectra of SiBEA and $Mo_{2.0}$SiBEA.

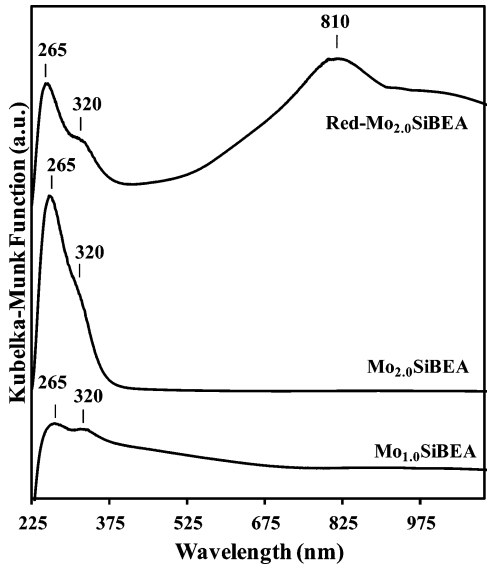

Figure 5. Ambient-atmosphere DR UV−vis spectra $Mo_{1.0}$SiBEA, $Mo_{2.0}$SiBEA, and Red-$Mo_{2.0}$SiBEA (treated with pure hydrogen at 943 K for 1 h).

(Scheme 1). This attribution is based on the simultaneous changes in the intensities of both UV−vis bands and data obtained for the system with vanadium reported in earlier works on V-containing zeolites.[37,38]

Moreover, the significant and simultaneous decreasing of the intensities of the bands at 265 and 320 nm upon reduction of $Mo_{1.0}$SiBEA and $Mo_{2.0}$SiBEA in a hydrogen stream at 943 K (Figure 5) confirms that these bands could be attributed to oxygen-to-mononuclear Mo(VI) charge-transfer transition involving oxygen in bridging (Mo—O—Si) and terminal (Mo═O) locations, respectively. The large band formed in the DR UV−vis spectrum of reduced $Mo_{2.0}$SiBEA, present in Figure 5 as an example and labeled Red-$Mo_{2.0}$SiBEA, between 550 and 850 nm is due to reduced Mo species such as Mo(V) (d^1) and/or Mo(IV) (d^2), in line with earlier works.[38,39] This

dx.doi.org/10.1021/jp410016g | J. Phys. Chem. C 2014, 118, 4143−4150

indicates that reduced Mo(V) and/or Mo(IV) is formed by treatment of $Mo_{1.0}$SiBEA and $Mo_{2.0}$SiBEA with H_2 at 943 K for 1 h.

3.3. EPR Evidence for the Formation of Isolated Mononuclear Mo(V). EPR spectroscopy was applied to gain additional information about molybdenum species formed in Mo_xSiBEA zeolite.

In the EPR spectrum of the as-prepared $Mo_{1.0}$SiBEA (Figures 6a and 7a), a signal related to paramagnetic Mo(V) is not observed, indicating that only Mo(VI) is present in this sample, in agreement with the DR UV−vis investigation discussed in section 3.2. However, the EPR spectrum of activated (outgassed under a vacuum) Act-$Mo_{1.0}$SiBEA zeolite at 298 K exhibits a large signal of axial symmetry typical of isolated mononuclear Mo(V) (Figures 6b and 7b) similar to those observed earlier for MoH-ZSM-5,[40] Mo/SAPO-11,[41] and PdMo/Y[42] zeolites. In addition, a much weaker isotropic signal was observed at g = 2.001 ($\sim g_e$) for Act-$Mo_{1.0}$SiBEA zeolite (Figures 6b and 7b), probably arising from a small amount of carbonaceous species, in line with earlier works on Mo/HZSM-5 and MoH-Beta zeolites.[43,44]

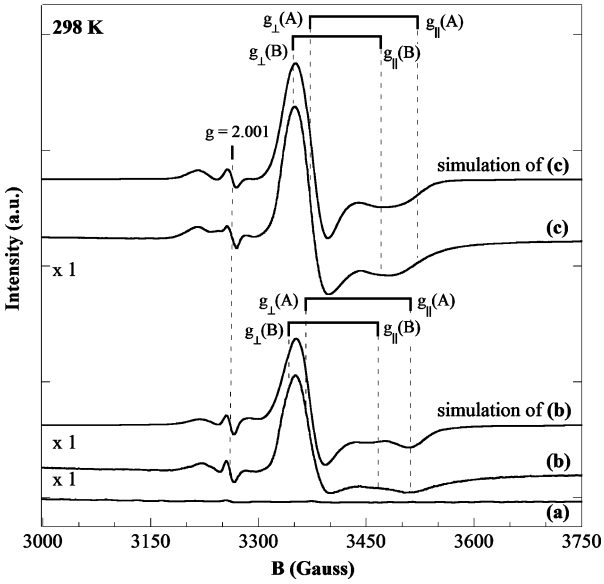

Figure 6. EPR spectra recorded at 298 K of (a) $M_{1.0}$SiBEA, (b) Act-$Mo_{1.0}$SiBEA, and (c) Red-Act-$Mo_{1.0}$SiBEA with simulations, where Act means activated (outgassed at 773 K for 2 h under vacuum) and Red means reduced (treated with pure hydrogen at 943 K for 1 h).

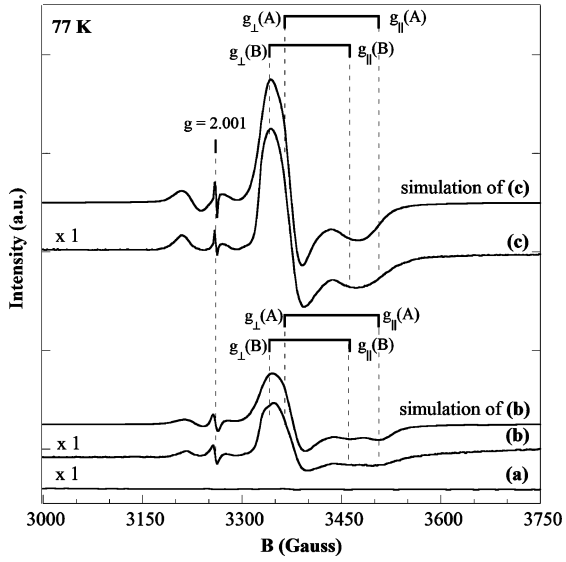

Figure 7. EPR spectra recorded using a 100-kHz field modulation and a 5-G standard modulation width at 77 K of (a) $M_{1.0}$SiBEA, (b) Act-$Mo_{1.0}$SiBEA, and (c) Red-Act-$Mo_{1.0}$SiBEA with signal simulations, where Act means activated (outgassed at 773 K for 2 h under vacuum) and Red means reduced (treated with pure hydrogen at 943 K for 1 h).

The appearance of the EPR signal of isolated Mo(V) in the spectrum of Act-$Mo_{1.0}$SiBEA suggests partial reduction of isolated mononuclear Mo(VI) to isolated mononuclear Mo(V) upon outgassing of $Mo_{1.0}$SiBEA (Scheme 1), consistent with the color change of the sample from white ($Mo_{1.0}$SiBEA) to pale blue (Act-$Mo_{1.0}$SiBEA).

The simulation of EPR spectra of Act-$Mo_{1.0}$SiBEA recorded at 298 and 77 K allows two species (A and B) with different EPR parameters corresponding to two different isolated mononuclear Mo(V) species to be distinguished (Figures 6b and 7b and Table 3). The order of the g-factor components of the two species ($g_e > g_\perp > g_\parallel$) is in agreement with a Mo(V) center surrounded by oxygen-containing ligands.[45] It has been shown[46] that the parallel component ($g_\parallel$) strongly increases with the coordination number of the molybdenyl moiety, from ∼1.75 for $Mo(V)_{4c}$ (tetracoordination) to ∼1.89 for $Mo(V)_{6c}$ (hexacoordination). Additionnaly, because of rapid relaxation, tetracoordinated Mo(V) was not visible at room temperature and required a temperature of 77 K or lower to be observed. In our case, both A and B species were observed at room temperature and 77 K with $g_\parallel$ s value of 1.86−1.87 and 1.88−1.89, respectively, which rules out of tetracoordinated Mo(V). However, both are consistent with either penta- or hexacoordinated Mo(V) species as follows: (i) pentacoordinated Mo(V) could represent O═Mo(—O—Si—)$_4$ or (O═)$_2$Mo(—O—Si—)$_3$ and (ii) hexacoordinated Mo(V) could represent O═Mo(—O—Si—)$_5$ or (O═)$_2$Mo(—O—Si—)$_4$.

Table 3. Simulated EPR Parameters of Molybdenum Species in $Mo_{1.0}$SiBEA

treatment	measured temp (K)	$g_\parallel$	$g_\perp$	$A_\parallel$ (G)	$A_\perp$ (G)
		Species A			
773 K, vacuum	77	1.858	1.935	110	40
	298	1.857	1.938	110	50
943 K, H_2	77	1.870	1.938	105	55
	298	1.864	1.936	100	55
		Species B			
773 K, vacuum	77	1.886	1.949	85	45
	298	1.882	1.947	85	35
943 K, H_2	77	1.887	1.951	95	50
	298	1.882	1.948	90	50

The EPR spectrum of Red-Act-$Mo_{1.0}$SiBEA recorded at 77 K looks similar to that of Act-$Mo_{1.0}$SiBEA recorded at both 298 and 77 K. As shown in Table 3, the g values of both A and B Mo(V) signals of Red-Act-$Mo_{1.0}$SiBEA recorded at 77 K are rather close to that of Act-$Mo_{1.0}$SiBEA recorded at both temperatures. Both signals are about 1.5−2 times more intense for Red-Act-$Mo_{1.0}$SiBEA than for Act-$Mo_{1.0}$SiBEA, indicating deeper reduction of Mo(VI) mononuclear species to Mo(V) upon H_2 treatment than during outgassing.

dx.doi.org/10.1021/jp410016g | J. Phys. Chem. C 2014, 118, 4143−4150

3.4. Reducibility of the Molybdenum Species. The reducibility of the molybdenum in $Mo_{1.0}$SiBEA and $Mo_{2.0}$SiBEA was investigated by temperature-programmed reduction (TPR) under flowing hydrogen (5% H_2 in Ar). Generally, according to the literature,[47,48] for Mo-containing zeolites, reduction of Mo(VI) takes place in two steps. First, MoO_3 species are reduced to MoO_2 species, and after that, Mo^{4+} ions are reduced to Mo(0). However, in our case, Mo occurs mainly as a well-dispersed species incorporated into the zeolite framework, which is much more difficult to reduce than extraframework polynuclear species.

As shown in Figure 8, the TPR patterns of $Mo_{1.0}$SiBEA and $Mo_{2.0}$SiBEA contain three peaks at 805, 870, and 1030−1040

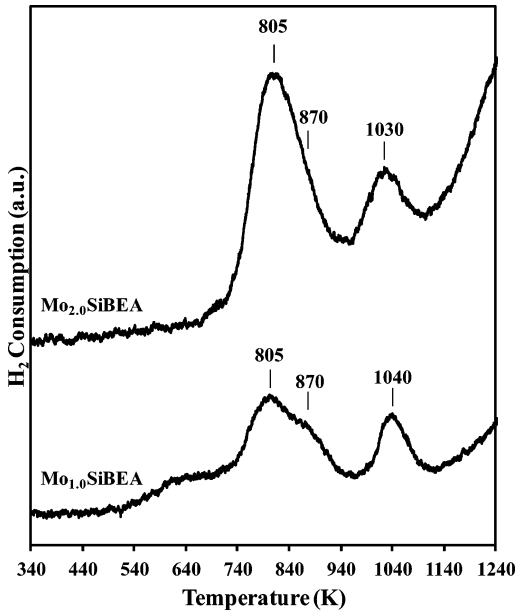

Figure 8. TPR experiment of H_2 consumption (5% H_2/Ar) for $M_{1.0}$SiBEA and $M_{2.0}$SiBEA in the temperature range of 298−1240 K.

K. The first two peaks could be attributed to reduction of two kinds of isolated mononuclear Mo(VI) into isolated mononuclear Mo(V) and/or Mo(IV). The third high-temperature reduced peak at 1030−1040 K is probably related to partial reduction of isolated mononuclear Mo(V) and/or Mo(IV) to Mo(0). The final reduction peak appears above 1240 K. It is probably related to reduction of Mo(IV) to Mo(0) strongly bonded to the zeolite framework and the most difficult to reduce, similarly to observations for Mo/HZSM-5 zeolite by Martínez et al.[49] and Jiang et al.[50]

3.5. TEM Results. Transmission electron microscopy experiments were carried out to show the influence of preparation conditions on the distribution and state of Mo nanoparticles after the reduction of $Mo_{2.0}$SiBEA.

TEM images of reduced $Mo_{2.0}$SiBEA are shown in Figure 9. These TEM images and the histogram of the particle size distribution reveal a uniform distribution of Mo nanoparticles in $Mo_{2.0}$SiBEA zeolite with an average size of 1.8 nm. These nanoparticles might be related to the presence of metallic Mo(0), which is line with earlier work on PdMo/Y-zeolite.[41]

The TEM results indicate that the mononuclear Mo(VI) species in MoSiBEA zeolite after reduction were transformed into nanoparticles of metallic Mo. The absence of Mo(0) nanoparticles larger than 4 nm indicates that the two-step

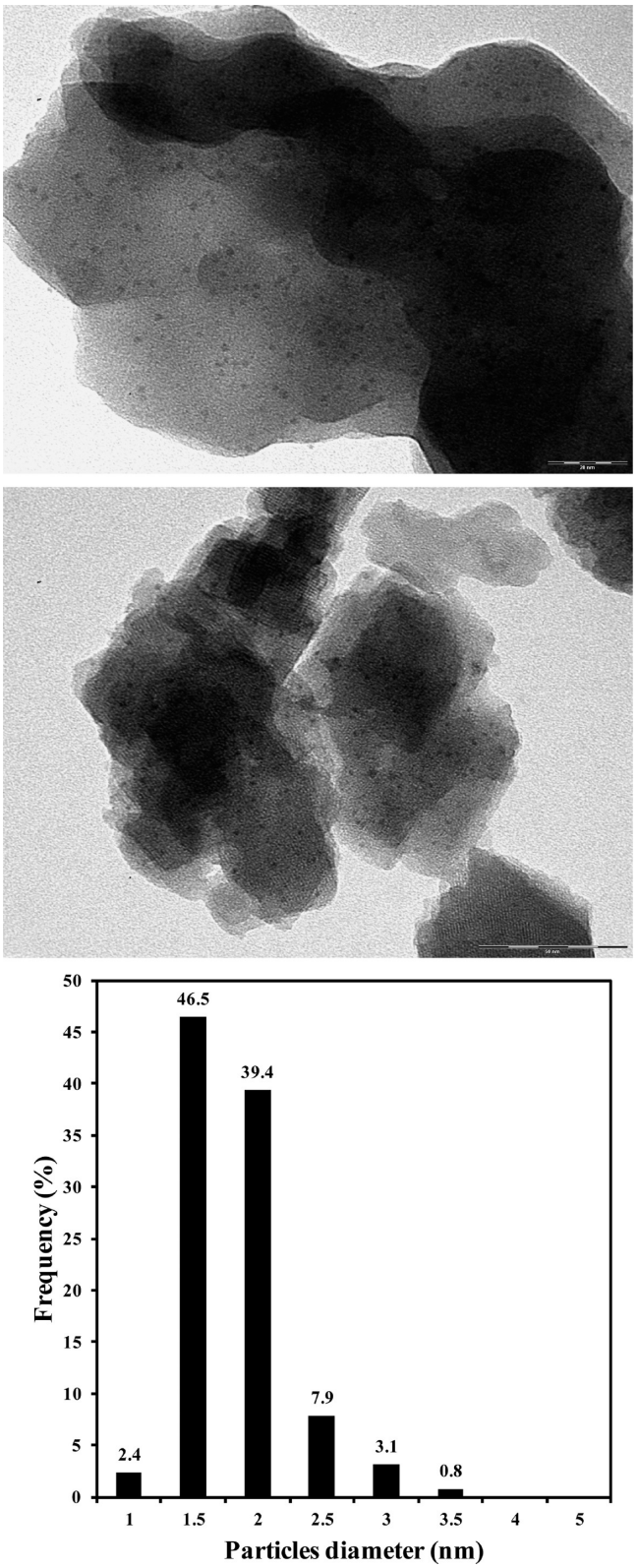

Figure 9. TEM images and histogram of the particle size distribution of Red-$Mo_{2.0}$SiBEA.

postsynthesis procedure applied in this work allows well-dispersed and small Mo(0) nanoparticles to be obtained throughout the pores of $Mo_{2.0}$SiBEA zeolite.

dx.doi.org/10.1021/jp410016g | J. Phys. Chem. C 2014, 118, 4143−4150

4. CONCLUSIONS

The two-step postsynthesis procedure applied in this work allows molybdenum to be incorporated into the vacant T-atom sites of the framework of SiBEA zeolite as an isolated mononuclear Mo(VI) species, as evidenced by the combined use of XRD and FTIR, NMR, and DR UV−visible spectroscopies.

The oxidation state of molybdenum in Mo_xSiBEA zeolite changes upon outgassing at 773 K for 2 h, as well as during treatment with hydrogen at 943 K for 1 h from the isolated mononuclear Mo(VI) to isolated mononuclear Mo(V) and/or Mo(IV) as evidenced by EPR and DR UV−vis investigations.

TPR patterns of Mo_xSiBEA contain three peaks at 805, 870, and 1030−1040 K. The first two peaks could be attributed to the reduction of two types of isolated mononuclear Mo(VI) species into two types of isolated mononuclear Mo(V) and/or Mo(IV) species. The third high-temperature reduced peak at 1030−1040 K could be attributed to the reduction of isolated mononuclear Mo(V) and/or Mo(IV) into Mo(0).

The formation of two kinds of isolated mononuclear Mo(V) species into reduced Mo_xSiBEA is evidenced by two EPR signals with different g and A parameters.

The Mo(0) nanoparticles obtained after reduction between 298 and 1240 K in a hydrogen stream (5% H_2/Ar) are very small (average size of 1.8 nm) and well-dispersed in the zeolite matrix as evidenced by TEM.

Further studies on Mo_xSiBEA zeolites are underway to determine their catalytic properties in methanol oxidation.

AUTHOR INFORMATION

Corresponding Author

*E-mail: stanislaw.dzwigaj@upmc.fr. Tel.: 33 1 44 27 21 13.

Notes

The authors declare no competing financial interest.

REFERENCES

(1) Hagen, J. *Industrial Catalysis*; Wiley-VCH Verlag GmbH & Co. KGaA: Weinheim, Germany, 2006.

(2) Frauwallner, M.-L.; López-Linares, F.; Lara-Romero, J.; Scott, C. E.; Ali, V.; Hernández, E.; Pereira-Almao, P. Toluene Hydrogenation at Low Temperature Using a Molybdenum Carbide Catalyst. *Appl. Catal. A* **2011**, *394*, 62−70.

(3) Guan, J.; Yang, G.; Zhou, D.; Zhang, W.; Liu, X.; Han, X.; Bao, X. Formation of Mo-Carbene Active Sites in Mo/Beta Zeolite Catalysts with Different Olefins: Theoretical Exploration of Possible Reaction Pathways and Substituent Effects. *Catal. Commun.* **2008**, *9*, 2213−2216.

(4) Vosmerikov, A. V.; Zaikovskii, V. I.; Korobitsyna, L. L.; Kozlov, V. V.; Arbuzova, N. V.; Zhuravkov, S. P. Methane Conversion into Aromatic Hydrocarbons over Ag−Mo/ZSM-5 Catalysts. *Kinet. Catal.* **2011**, *52*, 427−433.

(5) Vasenin, N. T.; Anufrienko, V. F.; Ismagilov, I. Z.; Larina, T. V.; Paukshtis, E. A.; Matus, E. V.; Tsikoza, L. T.; Kerzhentsev, M. A.; Ismagilov, Z. R. Effect of Thermal Treatment on States of Molybdenum in Mo/H-ZSM-5 Catalysts for Methane Dehydroaromatization: ESR and UV−Vis Study. *Top. Catal.* **2005**, *32*, 61−70.

(6) Brandhorst, M.; Cristol, S.; Capron, M.; Dujardin, C.; Vezin, H.; Le bourdon, G.; Payen, E. Catalytic Oxidation of Methanol on Mo/Al_2O_3 Catalyst: An EPR and Raman/Infrared Operando Spectroscopies Study. *Catal. Today* **2006**, *113*, 34−39.

(7) Tessonnier, J.-P.; Louis, B.; Ledoux, M.-J.; Pham-Huu, C. Green Catalysis for Production of Chemicals and CO-Free Hydrogen. *Catal. Commun.* **2007**, *8*, 1787−1792.

(8) Skutil, K.; Taniewski, M. Some Technological Aspects of Methane Aromatization (Direct and via Oxidative Coupling). *Fuel Process. Technol.* **2006**, *87*, 511−521.

(9) Borry, R. W., III; Kim, Y. H.; Huffsmith, A.; Reimer, J. A.; Iglesia, E. Structure and Density of Mo and Acid Sites in Mo-Exchanged H-ZSM5 Catalysts for Nonoxidative Methane Conversion. *J. Phys. Chem. B* **1999**, *103*, 5787−5796.

(10) Salama, T. M.; Othman, I.; Sirag, M.; El-Shobaky, G. A. Comparative Study of Molybdenum Oxide in NaY Zeolite Prepared by Conventional Impregnation and Vapor-phase Deposition Techniques. *Microporous Mesoporous Mater.* **2006**, *95*, 312−320.

(11) Sasaki, T.; Nakagawa, F.; Iwasawa, Y. Bound Site of Mo Atoms and Its Local Structure in a Mo/HY Catalyst Characterized by Extended X-ray Absorption Fine Structure and Density Functional Calculation. *J. Phys. Chem. B* **2005**, *109*, 2128−2138.

(12) Adam, F.; Iqbal, A. Silica Supported Amorphous Molybdenum Catalysts Prepared via Sol−Gel Method and Its Catalytic Activity. *Microporous Mesoporous Mater.* **2011**, *141*, 119−127.

(13) Mhamdi, M.; Ghorbel, A.; Delahay, G. Influence of the V + Mo/Al Ratio on Vanadium and Molybdenum Speciation and Catalytic Properties of V−Mo−ZSM-5 Prepared by Solid-State Reaction. *Catal. Today* **2009**, *142*, 239−244.

(14) Dzwigaj, S.; Janas, J.; Machej, T.; Che, M. Selective Catalytic Reduction of NO by Alcohols on Co- and Fe-Siβ Catalysts. *Catal. Today* **2007**, *119*, 133−136.

(15) Dzwigaj, S.; Peltre, M. J.; Massiani, P.; Davidson, A.; Che, M.; Sen, T.; Sivasanker, S. Incorporation of Vanadium Species in a Dealuminated β Zeolite. *Chem. Commun.* **1998**, 87−88.

(16) Dzwigaj, S.; Matsuoka, M.; Franck, R.; Anpo, M.; Che, M. Probing Different Kinds of Vanadium Species in the VSiβ Zeolite by Diffuse Reflectance UV−Visible and Photoluminescence Spectroscopies. *J. Phys. Chem. B* **1998**, *102*, 6309−6312.

(17) Dzwigaj, S. Recent Advances in the Incorporation and Identification of Vanadium Species in Microporous Materials. *Curr. Opin. Solid State Mater. Sci.* **2003**, *7*, 461−470.

(18) Dzwigaj, S.; Ivanova, E.; Kefirov, R.; Hadjiivanov, K.; Averseng, F.; Krafft, J. M.; Che, M. Remarkable Effect of the Preparation Method on the State of Vanadium in BEA Zeolite: Lattice and Extra-Lattice V Species. *Catal. Today* **2009**, *142*, 185−191.

(19) Spalek, T.; Pietrzyk, P.; Sojka, Z. Application of the Genetic Algorithm Joint with the Powell Method to Nonlinear Least-Squares Fitting of Powder EPR Spectra. *J. Chem. Inf. Model.* **2005**, *45*, 18−29.

(20) Higgins, J. B.; LaPierre, R. B.; Schlenker, J. L.; Rohrman, A. C.; Wood, J. D.; Kerr, G. T.; Rohrbaugh, W. J. The Framework Topology of Zeolite Beta. *Zeolites* **1988**, *8*, 446−452.

(21) Newsam, J. M.; Treacy, M. M. J.; Koetsier, W. T.; Degruyter, C. B. Structural Characterization of Zeolite Beta. *Proc. R. Soc. London, Ser. A.* **1988**, *420*, 375−405.

(22) Treacy, M. M. J.; Newsam, J. M. Two New Three-Dimensional Twelve-Ring Zeolite Frameworks of Which Zeolite Beta is a Disordered Intergrowth. *Nature* **1988**, *332*, 249−251.

(23) Sohn, J. R.; Park, J. H. Characterization of Dealuminated NiY Zeolite and Effect of Dealumination on Catalytic Activity for Ethylene Dimerization. *Appl. Catal. A* **2001**, *218*, 229−234.

(24) Rachwalik, R.; Olejniczak, Z.; Sulikowski, B. Dealumination of Ferrierite Type Zeolite: Physicochemical and Catalytic Properties. *Catal. Today* **2005**, *101*, 147−154.

(25) Hadjiivanov, K.; Penkova, A.; Kefirov, R.; Dzwigaj, S.; Che, M. Influence of Dealumination and Treatments on the Chromium Speciation in Zeolite CrBEA. *Microporous Mesoporous Mater.* **2009**, *124*, 59−69.

(26) Bourgeat-Lami, E.; Fajula, F.; Anglerat, D.; des Courières, T. Single Step Dealumination of Zeolite Beta Precursors for the Preparation of Hydrophobic Adsorbents. *Microporous Mater.* **1993**, *1*, 237−245.

(27) Janin, A.; Maache, M.; Lavalley, J. C.; Joly, J. F.; Raatz, F.; Szydlowski, N. FTIR Study of the Silanol Groups in Dealuminated HY Zeolites: Nature of the Extraframework Debris. *Zeolites* **1991**, *11*, 391−396.

(28) Dzwigaj, S.; Massiani, P.; Davidson, A.; Che, M. Role of Silanol Groups in the Incorporation of V in β Zeolite. *J. Mol. Catal. A* **2000**, *155*, 169−182.
(29) Beck, L. W.; Haw, J. F. Multinuclear NMR Studies Reveal a Complex Acid Function for Zeolite Beta. *J. Phys. Chem.* **1995**, *99*, 1076−1079.
(30) Woolery, G. I.; Alemany, L. B.; Dessau, R. M.; Chester, A. W. Spectroscopic Evidence for the Presence of Internal Silanols in Highly Siliceous ZSM-5. *Zeolites* **1986**, *6*, 14−16.
(31) Li, D.; Nishijima, A.; Morris, D. E. Zeolite-Supported Ni and Mo Catalysts for Hydrotreatments. I. Catalytic Activity and Spectroscopy. *J. Catal.* **1999**, *182*, 339−348.
(32) Prialiaud, H. Diffuse Reflectance Spectra of Molybdenum Ions Supported by Magnesia, γ-Alumina or Silica. *J. Less-Common Met.* **1977**, *54*, 387−399.
(33) Barrio, L.; Campos-Martín, J. M.; Pilar de Frutos, M.; Fierro, J. L. G. Alkene Epoxidation with Ethylbenzene Hydroperoxides Using Molybdenum Heterogeneous Catalysts. *Ind. Eng. Chem. Res.* **2008**, *47*, 8016−8024.
(34) Xiong, G.; Feng, Z.; Li, J.; Yang, Q.; Ying, P.; Xin, Q.; Li, C. UV Resonance Raman Spectroscopic Studies on the Genesis of Highly Dispersed Surface Molybdate Species on γ-Alumina. *J. Phys. Chem. B* **2000**, *104*, 3581−3588.
(35) Li, X.; Zhou, F.; Wang, A.; Wang, L.; Hu, Y. Influence of Templates on the Overgrowth of MCM-41 over HY and the Hydrodesulfurization Performances of the Supported Ni−Mo Catalysts. *Ind. Eng. Chem. Res.* **2009**, *48*, 2870−2877.
(36) de Lucas, A.; Valverde, J. L.; Rodriguez, L.; Sanchez, P.; Garcia, M. T. Partial Oxidation of Methane to Formaldehyde over Mo/HZSM-5 Catalysts. *Appl. Catal. A* **2000**, *203*, 81−90.
(37) Dzwigaj, S.; Matsuoka, M.; Anpo, M.; Che, M. Evidence of Three Kinds of Tetrahedral Vanadium (V) Species in VSiβ Zeolite by Diffuse Reflectance UV−Visible and Photoluminescence Spectroscopies. *J. Phys. Chem. B* **2000**, *104*, 6012−6020.
(38) Centi, G.; Perathoner, S.; Trifiro, F.; Aboukais, A.; Aïssi, C. F.; Guelton, M. Physicochemical Characterization of V-Silicalite. *J. Phys. Chem.* **1992**, *96*, 2617−2629.
(39) Prialiaud, H. In *Proceedings of the 2nd International Conference on Chemistry and Uses of Molybdenum*; Climax Molybdenum Co.: London, 1976; p 195.
(40) Kucherov, A. V.; Slinkin, A. A. Redox and Photo-Redox Properties of Isolated Mo^{5+} Ions in MoH-ZSM-5 and MoH-Beta Zeolites: In Situ ESR Study. *Catal. Lett.* **2000**, *64*, 53−57.
(41) Minming, H.; Johns, J. R.; Howe, R. F. EPR Study of the Superoxide Ion in Molybdenum Zeolites. *J. Phys. Chem.* **1988**, *92*, 1291−1295.
(42) Saïd Zina, M.; Ghorbel, A. Preparation and Characterization of Bimetallic PdMo/Y-Zeolite: Catalytic Properties in Methane Combustion. *Solid State Sci.* **2004**, *6*, 973−980.
(43) Ma, D.; Shu, Y.; Bao, X.; Xu, Y. Methane Dehydroaromatization under Nonoxidative Conditions over Mo/HZSM-5 Catalysts: EPR Study of the Mo Species on/in the HZSM-5 Zeolite. *J. Catal.* **2000**, *189*, 314−325.
(44) Ha, V. T. T.; Sarıoglan, A.; Erdem-Senatalar, A.; Ben Taârit, Y. An EPR and NMR Sudy on Mo/HZSM-5 Catalysts for the Aromatization of Methane: Investigation of the Location of the Pentavalent Molybdenum. *J. Mol. Catal. A* **2013**, *378*, 279−284.
(45) Che, M.; Fournier, M.; Launay, J. P. The Analog of Surface Molybdenyl Ion in Mo/SiO_2 Supported Catalysts: The Isopolyanion $Mo_6O_{19}^{3-}$ Studied by EPR and UV−Visible Spectroscopy. Comparison with Other Molybdenyl Compounds. *J. Chem. Phys.* **1979**, *71* (4), 1954−1960.
(46) Louis, C.; Che, M. EPR Investigation of the Coordination Sphere of Mo^{5+} Ions on Thermally Reduced Silica-Supported Molybdenum Catalysts Prepared by the Grafting Method. *J. Phys. Chem.* **1987**, *91*, 2875−2883.
(47) Song, Y.; Sun, C.; Shen, W.; Lin, L. Hydrothermal Post-Synthesis of HZSM-5 Zeolite to Enhance the Coke-Resistance of Mo/HZSM-5 Catalyst for Methane Dehydroaromatization Reaction: Reconstruction of Pore Structure and Modification of Acidity. *Appl. Catal. A* **2007**, *317*, 266−274.
(48) Jina, Z.; Liua, S.; Qina, L.; Liua, Z.; Wanga, Y.; Xiea, Z.; Wang, X. Methane Dehydroaromatization by Mo-Supported MFI-Type Zeolite with Core−Shell Structure. *Appl. Catal. A* **2013**, *453*, 295−301.
(49) Martínez, A.; Peris, E.; Derewinski, M.; Burkat-Dulak, A. Improvement of Catalyst Stability during Methane Dehydroaromatization (MDA) on Mo/HZSM-5 Comprising Intracrystalline Mesopores. *Catal. Today* **2011**, *169*, 75−84.
(50) Jiang, H.; Wang, L.; Cui, W.; Xu, Y. Study on the Induction Period of Methane Aromatization over Mo/HZSM-5: Partial Reduction of Mo Species and Formation of Carbonaceous Deposit. *Catal. Lett.* **1999**, *57*, 95−102.